Dalton Transactions

PAPER

View Article Online
View Journal | View Issue

Cite this: *Dalton Trans.*, 2014, **43**, 7290

Phase evolution and microwave dielectric properties of $xBi_{2/3}MoO_4-(1-x)BiVO_4$ ($0.0 \leq x \leq 1.0$) low temperature firing ceramics

Di Zhou,*[a] Wen-Bo Li,[a] Li-Xia Pang,[b] Jing Guo,[a] Ze-Ming Qi,[c] Tao Shao,[c] Xi Yao[a] and Clive A. Randall[d]

Received 8th December 2013,
Accepted 20th February 2014

DOI: 10.1039/c3dt53447b

www.rsc.org/dalton

In the present work, a full range of compositions of $xBi_{2/3}MoO_4-(1-x)BiVO_4$ ($0.0 \leq x \leq 1.0$) was prepared by the solid state reaction method. All the ceramic compositions could be readily densified to below 850 °C. As the x value increased, the monoclinic scheelite structure continuously changed to a tetragonal structure at $x = 0.10$, which means the ferroelastic phase transition temperature was lowered to near room temperature. In the compositional range $0.50 \leq x < 0.70$, a novel ordered scheelite phase was formed, most likely through A-site vacancy ordering. For compositions $x \geq 0.70$, a composite two-phase region consisting of the ordered scheelite and $Bi_{2/3}MoO_4$ phases was formed. High microwave permittivity around 75 and Qf values around 8000 GHz could be obtained in the compositions near the phase boundaries between monoclinic and tetragonal scheelite phases. The intrinsic microwave dielectric properties were extrapolated from the far infrared reflectivity spectra, and it was found that the polarization was dominated by the Bi–O stretches when $x \leq 0.10$.

I. Introduction

With the rapid development of mobile communication, satellite communication, Global Position System (GPS) and Wireless Local Area Network (WLAN) technology, low temperature co-fired ceramic (LTCC) technology has played an important role in the fabrication of microwave devices to meet the requirements of miniaturization and integration, due to its advantage in designing every layer separately and co-firing the dielectric and electrode layers together.[1–3]

Usually, most traditional microwave dielectrics with high performance have high sintering temperature and cannot be employed in LTCC technology. Over the last couple of decades, there has been a large amount of work carried out to lower the sintering temperature of high temperature sintered microwave dielectric ceramics. Besides the addition of sintering aids and the usage of ultra-fine initial powders, a novel, fruitful approach is to search for new compounds with intrinsic low sintering temperatures.[4–6]

Bismuth-based microwave dielectric ceramics have attracted much attention due to their low intrinsic sintering temperature and large permittivity (polarizability of Bi^{3+} is 6.12 Å^3).[7,8] The two classic bismuth-based microwave dielectric ceramics with pyrochlore-related structures are $(Bi_{1.5}Zn_{0.5})(Zn_{0.5}Nb_{1.5})O_7$ (α-BZN) and $Bi_2(Zn_{2/3}Nb_{4/3})O_7$ (β-BZN),[9,10] which can be densified at ~960 °C with high permittivity of 160 and 80, respectively. However, these pyrochlores have a relatively low quality factor (Qf = 300 GHz and 4000 GHz, respectively), limiting their application in microwave devices. Besides, the high sintering temperature (above 960 °C) also caused the volatilization of bismuth in ceramics. The traditional $BiVO_4$ material is used as an important kind of yellow dye in place of former lead chromium yellow with heavy metal content, which is harmful to humans.[11] Recently, $BiVO_4$ with distorted monoclinic scheelite structure has also attracted attention due to its high performance microwave properties (permittivity ~68, Qf ~8000 GHz) and low intrinsic sintering temperature below 900 °C, which put the volatilization problem under control.[7] The $BiVO_4$ material was reported to undergo a reversible second order ferroelastic phase transition (monoclinic scheelite ↔ tetragonal scheelite), which can be induced by a high temperature of about 255 °C or high pressure of about 16 kbar.[12,13] It was found that this phase transition can also be achieved by introducing larger ions than V^{5+} at the B-site, and

[a]*Electronic Materials Research Laboratory, Key Laboratory of the Ministry of Education & International Center for Dielectric Research, Xi'an Jiaotong University, Xi'an 710049, Shaanxi, China. E-mail: zhoudi1220@gmail.com; Fax: +86-29-82668679; Tel: +86-29-82668679*
[b]*Micro-optoelectronic Systems Laboratories, Xi'an Technological University, Xi'an 710032, Shaanxi, China*
[c]*National Synchrotron Radiation Laboratory, University of Science and Technology of China, Hefei, Anhui 230029, China*
[d]*The Pennsylvania State University, Center for Dielectric Studies, Materials Research Institute, University Park, PA 16802, USA*

the phase transition temperature can be lowered to near room temperature, as shown in our recent research.[6,14,15] Furthermore, excellent microwave dielectric properties can be reached in the compositions near the phase boundary, such as $[(Li_{0.5}Bi_{0.5})_{0.098}Bi_{0.902}][Mo_{0.098}V_{0.902}]O_4$ ceramic sintered at 650 °C with permittivity ~81 and Qf ~8000 GHz, and 0.1Bi$(Fe_{1/3}Mo_{2/3})O_4$–0.9BiVO_4 sintered at 820 °C with permittivity ~74.8 and Qf ~11 600 GHz.[6,16]

The general formula for scheelite ($CaWO_4$) oxides is ABO_4, in which the A cation is octahedrally coordinated to oxygen, while the B cation is tetrahedrally coordinated, and crystal structure details can be found in the literature.[14,17] It was reported that large concentrations of metal vacancy point defects could be introduced to A-sites when donor doped, D, with a trivalent cation, for example, and so the general chemical formula for scheelite becomes $(A^{+2}_{1-3x/2}D^{+3}_{x})BO_4$. For the special case of $x = 2/3$, we have a maximum of 1/3 vacancies on the A-site, assuming full ionic compensation with the donor and the metal vacancies, $[D^{\bullet}] = 2[Vm'']$. Such an example is $La_{2/3}MoO_4$, which shows disordered vacancy distribution when quenched from high temperatures, and ordered cation vacancies upon naturally cooling the sample. In this case, the MoO_4 tetrahedra were more distorted than those in the ideal tetragonal scheelite structure.[17–19] Similarly, in the case of pure $Bi_{2/3}MoO_4$, the A-site vacancies take on an ordered arrangement, and it was indexed in a scheelite related monoclinic structure with space group $P2_1/c$.[20,21] In our previous work, the $Bi_{2/3}MoO_4$ ($Bi_2Mo_3O_{12}$) ceramic was found to possess a microwave dielectric permittivity ~19, a Qf value ~21 800 GHz and an ultra-low sintering temperature around 620 °C. Hence, in the present work, a full composition study of $xBi_{2/3}MoO_4$–$(1 - x)BiVO_4$ ($0.0 \leq x \leq 1.0$) was carried out, considering the phase transition, microwave dielectric properties, and their relationship with the crystal structure.

II. Experimental methods

Proportionate amounts of reagent-grade starting materials of Bi_2O_3 (>99%, Shu-Du Powders Co. Ltd, Chengdu, China), V_2O_5 (>99%, Sinopharm Chemical Reagent Co., Ltd, Shanghai, China), and MoO_3 (>99%, Fuchen Chemical Reagents, Tianjin, China) were measured according to the stoichiometric formulation $xBi_{2/3}MoO_4$–$(1 - x)BiVO_4$ ($0.0 \leq x \leq 1.0$) (abbreviated here as BVMx). Powders were mixed and milled for 4 h using a planetary mill (Nanjing Machine Factory, Nanjing, China) by setting the running speed at 150 rpm with zirconia balls (2 mm in diameter) as milling media. The powder mixture was then dried and calcined at 600–700 °C for 4 hours. The calcined powders were ball milled for 5 hours with a running speed of 200 rpm to obtain fine powders. Then the powders were pressed into cylinders (10 mm in diameter and 4–5 mm in height) in a steel die with 5 wt% PVA binder addition under a uniaxial pressure of 200 MPa. Samples were sintered in the temperature range from 620 °C to 830 °C for 2 hours. Room temperature XRD was performed using XRD with CuKa radiation (Rigaku D/MAX-2400 X-ray diffractometer, Tokyo, Japan). Prior to examination, sintered pellets were crushed to powder in a mortar and pestle. Diffraction patterns were obtained between 5–65° (2θ) at a step size of 0.02°. The specimens for transmission electron microscopy were prepared from the sintered pellets and examined using a JEOL 2100 TEM microscope operated at 200 kV. To examine the grain morphology, as-fired and fractured surfaces were examined by scanning electron microscopy (SEM) (JSM-6460, JEOL, Tokyo, Japan). The Raman spectra at room temperature were obtained on polished pellets with a Raman spectrometer (inVia, Renishaw, England), excited by an Ar^+ laser (514.5 nm). The high temperature Raman spectra were measured using another Raman spectrometer (LabRAM HR800, HORIBA Jobin Yvon, France). The room temperature infrared reflectivity spectra were measured using a Bruker IFS 66v FTIR spectrometer on an infrared beamline station (U4) at National Synchrotron Radiation Lab. (NSRL), China. Dielectric properties at microwave frequency were measured with the $TE_{01\delta}$ dielectric resonator method with a network analyzer (HP 8720 Network Analyzer, Hewlett-Packard) and a temperature chamber (Delta 9023, Delta Design, Poway, CA).

III. Results and discussion

The X-ray diffraction patterns for $xBi_{2/3}MoO_4$–$(1 - x)BiVO_4$ ($0.0 \leq x \leq 1.0$) ceramics sintered at different temperatures, the cell parameters as a function of x value, and the schematic structure of $BiVO_4$ and $Bi_{2/3}MoO_4$ with only half the unit cell shown in the *ab*-plane are presented in Fig. 1. As to be expected, based on our previous investigations on $(A_{0.5x}Bi_{1-0.5x})(Mo_xV_{1-x})O_4$ (A = Li, Na and K) and $xBi(Fe_{1/3}Mo_{2/3})O_4$–$(1 - x)BiVO_4$ systems,[6,14,15] as the x value increased from 0.02 to 0.10, small amounts of substitution with bigger ionic radius, such as Mo^{6+} and Fe^{3+} for V^{5+}, occur at the B-site of the ABO_4 composition. This results in the onset of a second order ferroelastic phase transition to tetragonal scheelite structure. Experimentally, the transition from monoclinic to tetragonal is noted by merging of X-ray powder diffraction peaks (1 0 1) and (0 1 1), (2 0 0) and (0 2 0), *etc.* As seen from Fig. 1(a), this is common, irrespective of vacancies or cation substitution at the A site. This ferroelastic phase transition is believed to result from the increase of the atomic packing factor in the monoclinic phase region, for which the cell volume is dominated by the tetrahedron BO_4 network. As the x value increased to 0.50, a few super-lattice diffraction peaks could be observed beside the peaks of tetragonal scheelite (marked inside boxes in Fig. 1(b)). When the x value increased to 0.70, a trace of the main peaks of monoclinic $Bi_{2/3}MoO_4$ phase at 28.13° and 29.26° could be revealed, which indicates that the solid solubility of the single-phase tetragonal materials reached a maximum here. As the x value further increased, the intensity of the tetragonal scheelite

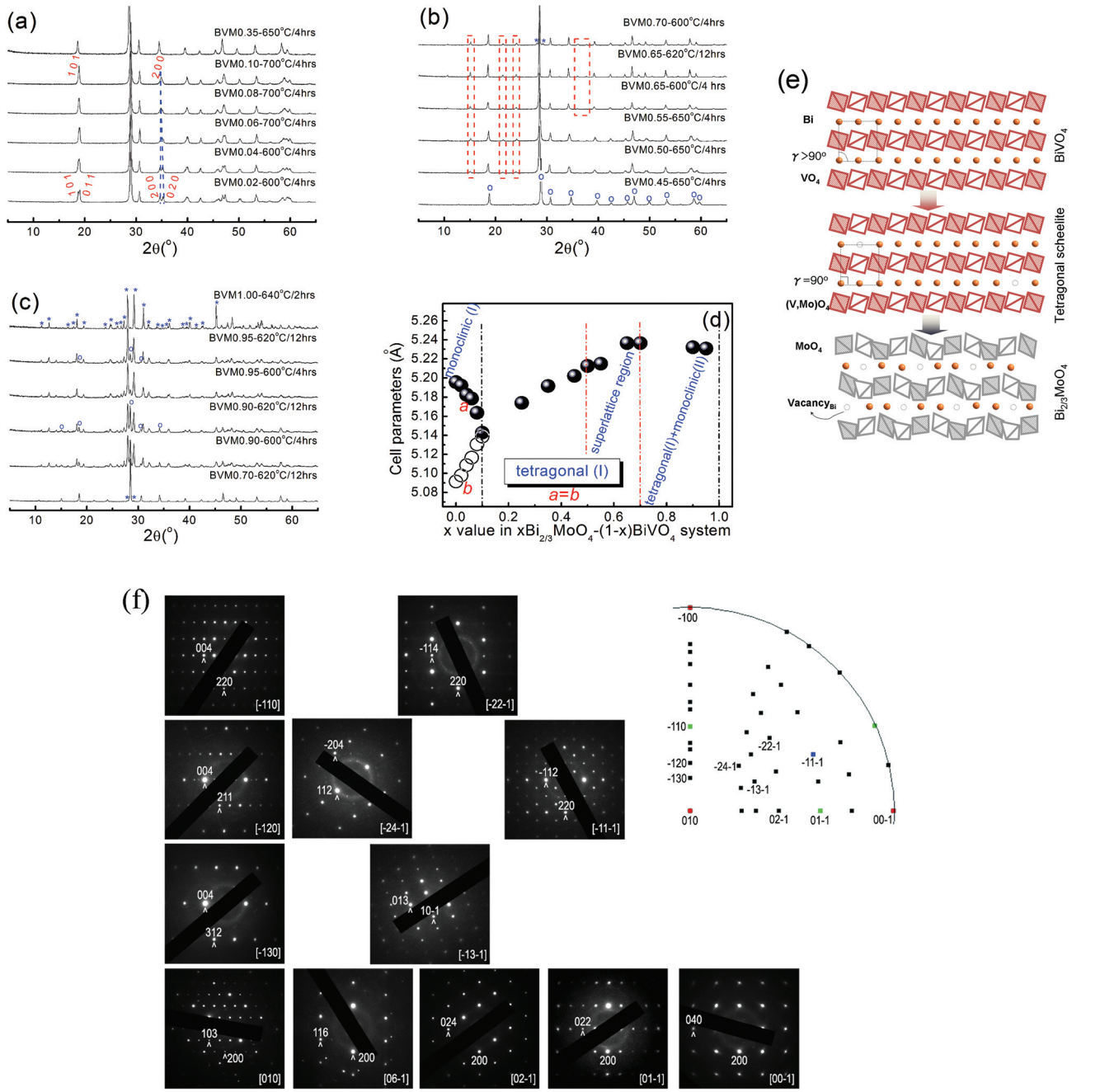

Fig. 1 X-ray diffraction patterns for $xBi_{2/3}MoO_4$–$(1-x)BiVO_4$ ($0.0 \leq x \leq 1.0$) ceramics sintered at different temperatures (a) (the merging of (1 0 1) and (0 1 1), (2 0 0) and (0 2 0) is marked by dash line), (b) (the super-lattice diffraction peaks were marked), and (c). (○: tetragonal scheelite phase, *: $Bi_{2/3}MoO_4$ monoclinic phase). (d) The cell parameters of scheelite phase as a function of x value (the four regions were distinguished by the cell parameters). (e) The schematic structure of $BiVO_4$ (top) and $Bi_{2/3}MoO_4$ (bottom) with only half the unit cell shown in the *ab*-plane. (f) A set of selected area electron diffraction patterns recorded from the BVM0.35 sample.

peaks decreased, and pure monoclinic $Bi_{2/3}MoO_4$ phase was formed at $x = 1.00$. It must be pointed out that the super-lattice peaks and phase composition in $xBi_{2/3}MoO_4$–$(1-x)$ $BiVO_4$ ($0.0 \leq x \leq 1.0$) ceramics were not influenced by annealing times, which indicates that the phase equilibrium can be easily reached here, and kinetics are relatively fast. Schematic diagrams of the ideal scheelite structure with vacancies less than 1/3 at the A-site and the pure monoclinic $Bi_{2/3}MoO_4$ phase are shown in Fig. 1(e). The phase transition from monoclinic to tetragonal scheelite structure can be attributed to the small amount of substitution of Mo^{6+} for V^{5+} on the B-site with disordering arrangement. Meanwhile, the A site vacancy also arranges in a disordering manner. In the super-lattice region ($x \geq 0.50$), the vacancy and Bi^{3+} cations arrange in an ordered

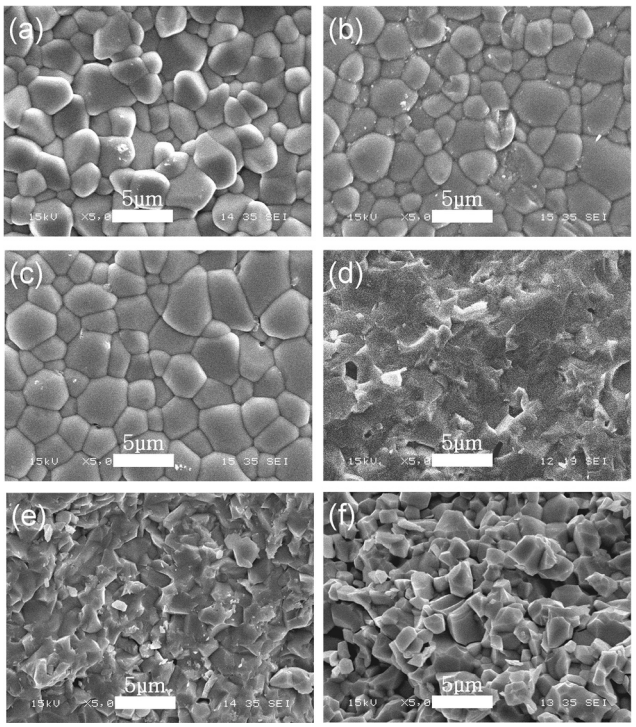

Fig. 2 SEM photos of as-fired surfaces of (a) BVM0.06 ceramic sintered at 830 °C/2 hours, (b) BVM0.08 ceramic sintered at 830 °C/2 hours, (c) BVM0.10 ceramic sintered at 780 °C/2 hours, and fractured surfaces of (d) BVM0.35 ceramic sintered at 680 °C/2 hours, (e) BVM0.65 ceramic sintered at 650 °C/2 hours, and (f) BVM1.00 ceramic sintered at 620 °C/2 hours.

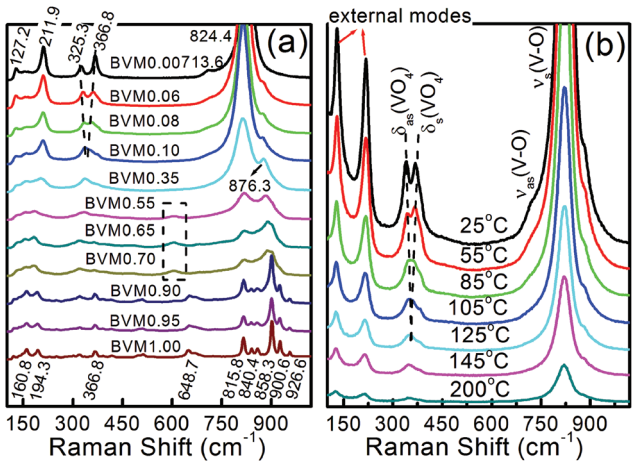

Fig. 3 (a) Room temperature Raman spectra of $xBi_{2/3}MoO_4$–$(1 - x)$ $BiVO_4$ ($0.0 \leq x \leq 1.0$) ceramics and (b) *in situ* Raman spectra of BVM0.06 sample in the temperature range 25 °C–200 °C.

manner, and it can still be tolerated under the tetragonal scheelite structure. The solid solubility of the vacancy of Bi^{3+} at the A-site reaches a maximum of about 23 mol% in the tetragonal scheelite structure at $x = 0.7$. With a further increase of x value, the tetragonal scheelite structure cannot hold any more vacancies, and a monoclinic $Bi_{2/3}MoO_4$ is formed to arrange the increasing Bi^{3+} vacancy. The maximum value of vacant A-site cations is 1/3 in the scheelite-related defect structures, which can be represented as $(A^{+2}{}_{1-3x/2}D^{+3}{}_x)BO_4$, and the MoO_4 here are somewhat more distorted than those in the ideal tetragonal $A^{+2}MoO_4$ scheelites. In particular, the MoO_4 tetrahedra in $Bi_{2/3}MoO_4$ reaches a most distorted situation, as seen in Fig. 1(e). A set of representative transmission electron diffraction patterns of selected areas of the BVM0.35 sample is shown in Fig. 1(f). All patterns were indexed according to a scheelite tetragonal unit cell with lattice parameters $a = b = 5.192$ Å and $c = 11.701$ Å, which correspond well with the XRD results.

SEM micrographs of as-fired and fractured surfaces demonstrate the granular microstructure of the $xBi_{2/3}MoO_4$–$(1 - x)$ $BiVO_4$ ceramics ($x = 0.06$, 0.08, 0.10, 0.35, 0.65, and 1.00) sintered at different temperatures, as shown in Fig. 2. Dense and homogeneous microstructures with almost no pores were revealed in all compositions. The densification temperature decreased almost linearly from 830 °C for BVM0.06 to about 620 °C for pure $Bi_{2/3}MoO_4$ ceramic. As seen from Fig. 2(d)–(f), the fractures changed gradually from a transgranular fracture to an intergranular one as the x value increased from 0.35 to 1.00. This might be attributed to the decreasing sintering temperature as the x value increased, and the low relative density of pure $Bi_{2/3}MoO_4$ ceramic, in which the pores can more easily promote the intergranular fracture.

The room temperature Raman spectra of $xBi_{2/3}MoO_4$–$(1 - x)BiVO_4$ ($0.0 \leq x \leq 1.0$) ceramics are shown in Fig. 3(a). Similar results to previous work are obtained here for pure $BiVO_4$.[14,15] The intense Raman band near 824.4 cm^{-1} is assigned to ν_s(V–O), and that with a weak shoulder at about 713.6 cm^{-1} is assigned to ν_{as}(V–O). The symmetric A_g bending mode of vanadate anion $\delta_s(VO_4{}^{3-})$ and the anti-symmetric B_g bending mode of vanadate anion $\delta_{as}(VO_4{}^{3-})$ modes are near 366.8 and 325.3 cm^{-1}, respectively, and external modes (rotation/translation) occur near 211.9 cm^{-1} and 127.2 cm^{-1}, respectively. Since ferroelastic phase transition can be induced here, the characteristic merging of the $\delta_s(VO_4)$ (B_g) and $\delta_{as}(VO_4)$ (A_g) modes at around 366.8 and 325.3 cm^{-1} for pure $BiVO_4$ to one at 340.2 cm^{-1} for BVM0.10 could be observed, which is similar to the our previous results.[6] The *in situ* Raman spectra of BVM0.06 sample in the temperature range 25–200 °C are shown in Fig. 3(b). It is observed that as the temperature increased, the $\delta_s(VO_4)$ and $\delta_{as}(VO_4)$ modes moved closer to each other, and finally became a single peak at about 105 °C. This result is consistent with the existence of the ferroelastic phase transition in the $xBi_{2/3}MoO_4$–$(1 - x)BiVO_4$ system and its dependence on both composition and temperature. For the pure $Bi_{2/3}MoO_4$, the sharp bands at 926.6, 900.6, 858.3, 840.4, 815.8, and 648.7 cm^{-1} are assigned to the Mo–O stretching modes, and the bands at 160.8, 194.3, and 366.8 cm^{-1} are assigned to the bending/wagging and external modes (and possible Bi–O stretches), which is similar to other reports in the literature.[22–24] In particular, the excellent

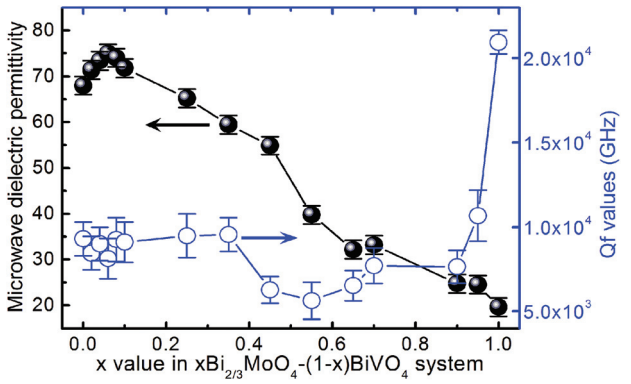

Fig. 4 Room temperature microwave dielectric permittivity and Qf values of $xBi_{2/3}MoO_4$–$(1-x)BiVO_4$ ($0.0 \le x \le 1.0$) ceramics as a function of x value.

work of Hardcastle and Wachs[22] considered detailed assignments of the Raman bands, and the relationship between Raman spectra, molybdenum coordinations, and Mo–O bond lengths. As the Mo content increased with x value, the Mo–O stretching band at around 876.3 cm^{-1} became stronger and replaced the V–O stretching band at 820 cm^{-1} as the new strongest one at x = 0.65. The Raman spectra are sensitive to the ordered structure, and a new band at around 604 cm^{-1} was observed for x = 0.55, 0.65, and 0.70 samples. Based on the Bi^{3+} vacancy ordering from XRD analysis, the band at 604 cm^{-1} is understandable and may be assigned to Bi–O stretches and medium-range order. For the BVM0.90 sample, it is seen that the spectra are mixtures of both BVM0.70 and BVM1.00, which further confirms the XRD results.

Fig. 4 shows the room temperature microwave dielectric properties of $xBi_{2/3}MoO_4$–$(1-x)BiVO_4$ ($0.0 \le x \le 1.0$) ceramics as a function of x value (at 4.8–8.5 GHz). The microwave permittivity first increased linearly from 69 to a maximum value of ~75 as the x value increased from 0.0 to 0.06, and then decreased down to 19.6 for the final member $Bi_{2/3}MoO_4$. This agrees well with the rule that the maximum value of permittivity can be obtained in the compositions near the phase boundary of monoclinic and tetragonal phases due to the decrease of the cell volume.[6,15] The Qf values remained stable at about 8000 GHz in the range $0.0 \le x \le 0.35$. Then it decreased to around 6000 GHz for x = 0.55, 0.65, and 0.70, and this might be attributed to the ordered arrangement of Bi^{3+} vacancies. Finally, the Qf value increased sharply from 8000 GHz for BVM0.90 to around 21 000 GHz for the pure $Bi_{2/3}MoO_4$ ceramic.

The temperature dependence of microwave dielectric permittivity and Qf value of $xBi_{2/3}MoO_4$–$(1-x)BiVO_4$ (x = 0.06, x = 0.08, x = 0.10, and x = 0.35) ceramics are shown in Fig. 5. It can be seen that the expected maximum value of relative permittivity as a function of temperature could be observed in samples with x = 0.06, x = 0.08, and x = 0.10, which means that the ferroelastic phase transition temperature in $xBi_{2/3}MoO_4$–$(1-x)BiVO_4$ ceramics decreased from 113 °C at x = 0.06 to 29 °C at x = 0.10. When the x value increased to 0.35, no obvious peak is observed, even when the temperature is as low as −250 °C and the microwave dielectric permittivity almost decreased linearly with an increase in the temperature, which means that the monoclinic scheelite structure cannot be formed in this composition. This result is also similar to the situation in the $xBi(Fe_{1/3}Mo_{2/3})O_4$–$(1-x)BiVO_4$ system.[6] It seems that the Qf values decreased sharply with the temperature when $x \le 0.10$ and the introduction of $Bi_{2/3}MoO_4$ improves the temperature stability of the Qf value.

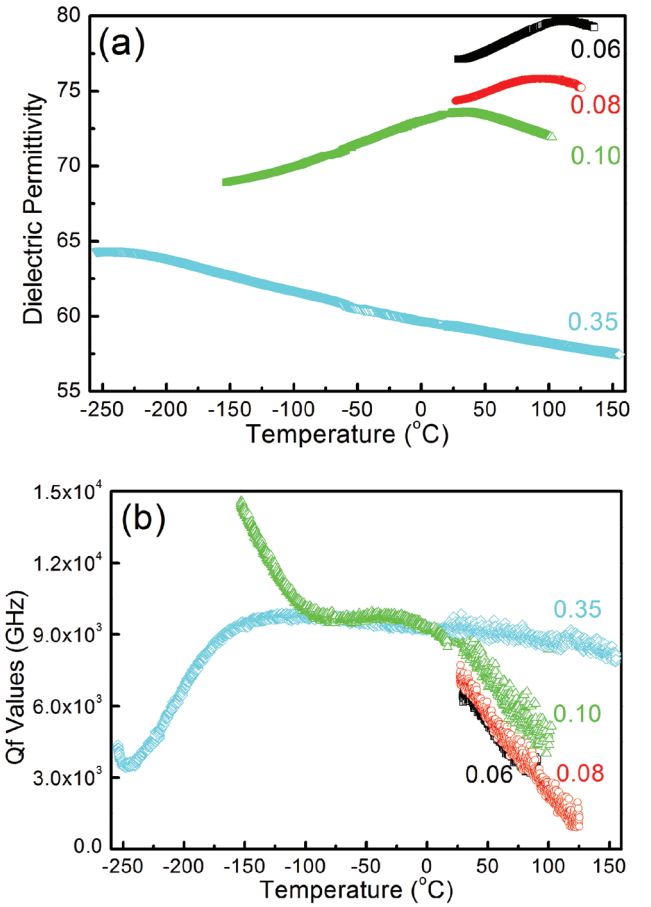

Fig. 5 Microwave dielectric permittivity (a) and Qf value (b) of $xBi_{2/3}MoO_4$–$(1-x)BiVO_4$ (x = 0.06, x = 0.08, x = 0.10 and x = 0.35) ceramics as a function of temperature (–260 °C to +150 °C).

Fig. 6 presents the room temperature IR reflectivity spectra of $xBi_{2/3}MoO_4$–$(1-x)BiVO_4$ ($0.0 \le x \le 1.0$) ceramics. It is seen that the two bands at 316 cm^{-1} and 357 cm^{-1}, which are assigned to $\delta_{as}(VO_4)$ mode and $\delta_s(VO_4)$, respectively, moved closer to each other with the increase of x value and finally merged into one band at around x = 0.10. Furthermore, the bands below 200 cm^{-1} (at least three) for pure $BiVO_4$ broadened and gradually overlapped with the increase of x value, and then could not be distinguished from each other at x = 0.10. All these phenomena reflect the increase of the degree of symmetry.

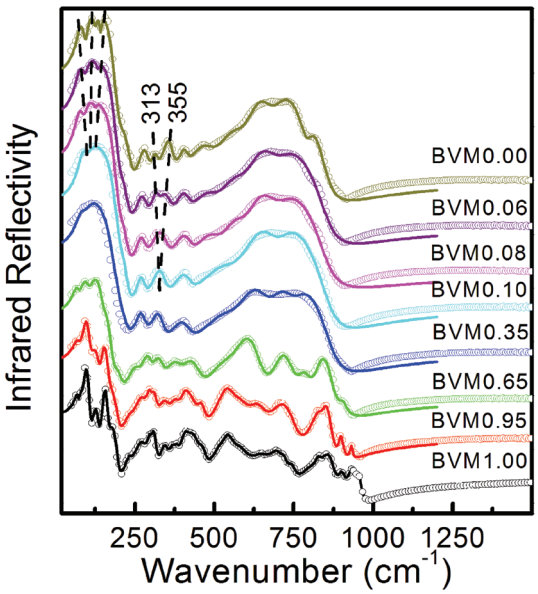

Fig. 6 Measured and calculated infrared reflectivity spectra of the $x\mathrm{Bi}_{2/3}\mathrm{MoO}_4$–$(1-x)\mathrm{BiVO}_4$ ($0.0 \le x \le 1.0$) ceramics (solid line for fitting values and circle for measured values).

To further study the intrinsic microwave dielectric properties, the IR reflectivity spectra of $x\mathrm{Bi}_{2/3}\mathrm{MoO}_4$–$(1-x)\mathrm{BiVO}_4$ ($0.0 \le x \le 1.0$) ceramics were analyzed using a classical harmonic oscillator model as follows:

$$\varepsilon^*(\omega) = \varepsilon_\infty + \sum_{j=1}^{n} \frac{{\omega_{pj}}^2}{{\omega_{oj}}^2 - \omega^2 - j\gamma_j\omega} \quad (1)$$

where $\varepsilon^*(\omega)$ is the complex dielectric function; ε_∞ is the dielectric constant caused by the electronic polarization at high frequencies; γ_j, ω_{oj}, and ω_{pj} are the damping factor, the transverse frequency, and plasma frequency of the jth Lorentz oscillator, respectively; and n is the number of transverse phonon modes. The complex reflectivity $R(\omega)$ can be written as:

$$R(\omega) = \left|\frac{1-\sqrt{\varepsilon^*(\omega)}}{1+\sqrt{\varepsilon^*(\omega)}}\right|^2 \quad (2)$$

The fitted IR reflectivity values are shown in Fig. 6, and the complex permittivities are shown in Fig. 7. It is seen that all the calculated dielectric permittivity and dielectric loss values are almost equal to the measured ones using $\mathrm{TE}_{01\delta}$ method, which implies that the majority of the dielectric contribution for this system in the microwave region was attributed to the absorption of structural phonon oscillation in the infrared region and very little contribution from defect phonon scattering. The phonon parameters obtained from the fitting of the infrared reflectivity spectra of $x\mathrm{Bi}_{2/3}\mathrm{MoO}_4$–$(1-x)\mathrm{BiVO}_4$ (x = 0.00, x = 0.06, x = 0.08, and x = 0.10) ceramics are listed in Tables 1 and 2. It can be seen that the dielectric polarization contribution from the vibration modes below 150 cm^{-1} can reach above 75% of the total value for x = 0.00, 0.06, 0.08, and 0.10 sample, and it is quite different from the result of pure $\mathrm{Bi}_{2/3}\mathrm{MoO}_4$ (about 5% from the first mode, the detailed data are not shown here). This implies that the dielectric polarization contribution of monoclinic scheelite solid solution comes from the external modes, which means the vibrational modes of Bi–O stretches. However, due to the overlapping of modes at low wave number, the accuracy of calculated permittivity was influenced by the errors from the fitting. It is understandable that the neighboring structure of Bi^{3+} can account for the change of macroscopical permittivity due to its large polarization about 6.12 $\mathrm{Å}^3$, which is much larger than that of Mo^{6+} and V^{5+} ions (3.28 $\mathrm{Å}^3$ and 2.92 $\mathrm{Å}^3$, respectively). Hence, although the overlapping of $\delta_{as}(\mathrm{VO}_4)$ mode and the $\delta_s(\mathrm{VO}_4)$, corresponding to the ferroelastic phase transition, can be obviously observed both from Raman and IR spectra, their

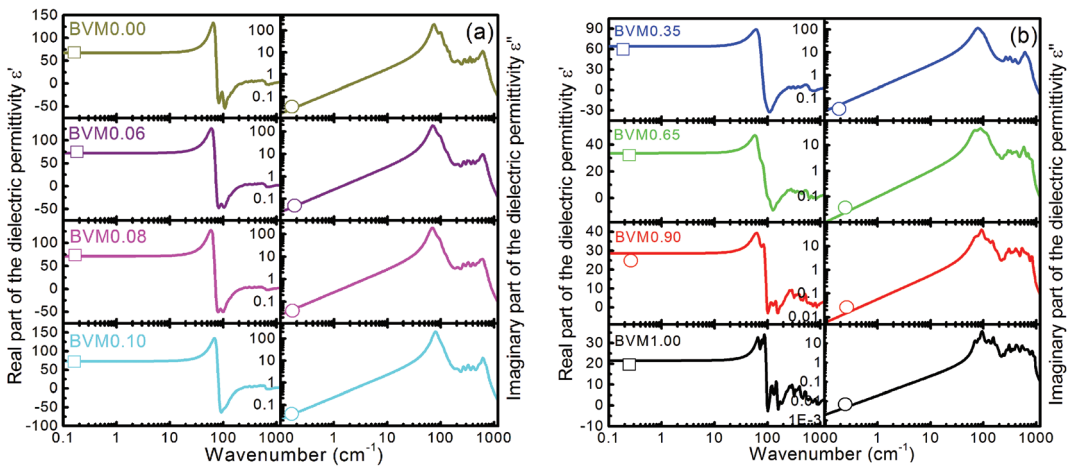

Fig. 7 Calculated and measured complex permittivity of the $x\mathrm{Bi}_{2/3}\mathrm{MoO}_4$–$(1-x)\mathrm{BiVO}_4$ ($0.0 \le x \le 1.0$) ceramics for (a) x = 0.00, 0.06, 0.08, 0.10 and (b) x = 0.35, 0.65, 0.90, 1.00.

Table 1 Phonon parameters obtained from the fitting of the infrared reflectivity spectra of $x Bi_{2/3}MoO_4$–$(1-x)BiVO_4$ (x = 0.00 and 0.060) ceramics

Mode	ω_{oj}	ω_{pj}	γ_j	$\Delta\varepsilon_j$	Mode	ω_{oj}	ω_{pj}	γ_j	$\Delta\varepsilon_j$
1	75.09	509.75	18.80	46.1	1	72.32	536.12	22.58	55
2	101.18	334.49	17.97	10.9	2	98.16	289.03	24.39	8.67
3	127.16	111.26	12.06	0.77	3	135.49	75.47	14.60	0.31
4	144.34	84.72	8.88	0.35					
5	213.18	182.22	57.50	0.73	4	211.63	232.38	50.06	0.39
6	280.06	183.40	34.41	0.43	5	272.86	184.21	40.46	0.46
7	315.59	124.98	23.30	0.16	6	317.58	134.63	24.46	0.18
8	356.92	240.33	33.32	0.45	7	346.42	224.71	47.32	0.42
9	407.15	173.49	29.96	0.18	8	406.43	229.45	45.14	0.32
10	472.24	371.50	85.37	0.62	9	482.32	350.23	94.85	0.52
11	560.48	477.86	86.15	0.73	10	565.87	450.3	91.65	0.63
12	625.27	693.64	82.15	1.23	11	630.24	672.97	95.66	1.14
13	696.63	403.49	89.51	0.34	12	711.71	411.74	12 244	0.34
14	799.23	149.46	46.86	0.04					
x = 0.00	ε_∞ = 3.95		ε_0 = 63.03		x = 0.06	ε_∞ = 3.59		ε_0 = 68.38	

Table 2 Phonon parameters obtained from the fitting of the infrared reflectivity spectra of $x Bi_{2/3}MoO_4$–$(1-x)BiVO_4$ (x = 0.08 and 0.10) ceramics

Mode	ω_{oj}	ω_{pj}	γ_j	$\Delta\varepsilon_j$	Mode	ω_{oj}	ω_{pj}	γ_j	$\Delta\varepsilon_j$
1	70.57	524.74	21.56	55.3	1	81.08	610.30	23.34	56.70
2	94.31	275.34	23.39	8.52	2	106.02	272.35	31.18	6.60
3	127.34	69.07	15.13	0.29					
4	210.69	126.04	49.34	0.36	3	209.86	135.68	50.04	0.42
5	269.37	172.38	37.23	0.41	4	270.22	170.28	32.68	0.40
6	329.01	278.83	57.22	0.72	5	329.60	267.83	46.71	0.66
7	404.65	272.83	57.89	0.46	6	407.65	293.72	59.98	0.52
8	487.02	369.92	92.81	0.58					
9	562.43	446.24	88.24	0.63	7	531.67	488.90	120.98	0.85
10	624.43	572.97	95.54	0.84	8	627.85	845.65	101.39	1.81
11	710.39	338.38	119.96	0.23	9	714.65	475.56	109.01	0.44
x = 0.08	ε_∞ = 3.05		ε_0 = 68.34		x = 0.10	ε_∞ = 4.41		ε_0 = 68.40	

dielectric polarization contribution to the microwave permittivity were quite low, and their influence could be ignored.

IV. Conclusions

The full compositional range of $x Bi_{2/3}MoO_4$–$(1-x)BiVO_4$ ($0.0 \leq x \leq 1.0$) ceramics were prepared *via* the solid state reaction method. The phase diagram of the whole system can be separated into at least four regions in the temperature below the melting points: I, scheelite monoclinic phase region with $0.0 \leq x \leq 1.0$; II, scheelite tetragonal phase region with $0.1 < x < 0.5$; III, an ordered scheelite phase region with $0.5 \leq x < 0.7$; IV, composite phase region with $0.7 \leq x < 1.0$ (ordered scheelite and monoclinic $Bi_{2/3}MoO_4$ phase). The characteristic overlapping of $\delta_s(VO_4)$ (B_g) and $\delta_{as}(VO_4)$ (A_g) modes during the ferroelastic phase transition could be observed in Raman spectra. Excellent microwave dielectric properties with permittivity around 75 and Qf value around 8000 GHz could be obtained in the compositions near the phase boundary (x = 0.10) of monoclinic and tetragonal scheelite phases. It can be concluded that the polarization contribution in the microwave region is dominated by the Bi–O stretches in $x Bi_{2/3}MoO_4$–$(1-x)BiVO_4$ ($0.0 \leq x \leq 1.0$) when $x \leq 0.10$ from the intrinsic results calculated from the fitting data of far infrared spectra. Hence, it would be an effective way to improve the microwave dielectric properties of bismuth based scheelite ceramics by modifying the A-site occupation and ions.

Acknowledgements

This work was supported by National Science Foundation of China (51202182, 51202178), the Fundamental Research Funds for the Central University, the international cooperation project of Shaanxi Province (2013KW12-04), the State Key Laboratory of New Ceramic and Fine Processing Tsinghua University and the 111 Project of China (B14040). The author would like to thank Qiu-Ping Wang, Han-Chen Liu, and Chao Zhou for their help in Raman experimental and the administrators in IR beamline workstation of National Synchrotron Radiation Laboratory (NSRL) for their help in the IR measurement. The SEM work was partially done at International Center for Dielectric Research (ICDR), Xi'an Jiaotong University, Xi'an, China and the authors thank Ms. Lu Lu and Ms. Yan-Zhu Dai for their help with TEM and SEM. We also wish to thank the National Science Foundation I/UCRC program, as part of the Center for Dielectric Studies under Grant No. 0628817, for

partial support and also the MCL facilities at Penn State University.

References

1 M. T. Sebastian and H. Jantunen, *Int. Mater. Rev.*, 2008, **53**, 57.
2 R. J. Cava, *J. Mater. Chem.*, 2001, **11**, 54.
3 D. Zhou, H. Wang, L. X. Pang, C. A. Randall and X. Yao, *J. Am. Ceram. Soc.*, 2009, **92**, 2242.
4 D. K. Kwon, M. T. Lanagan and T. R. Shrout, *J. Am. Ceram. Soc.*, 2005, **88**, 3419.
5 M. Udovic, M. Valant and D. Suvorov, *J. Am. Ceram. Soc.*, 2004, **87**, 591.
6 D. Zhou, L. X. Pang, J. Guo, Z. M. Qi, T. Shao, X. Yao and C. A. Randall, *J. Mater. Chem.*, 2012, **22**, 21412.
7 M. Valant and D. Suvorov, *J. Am. Ceram. Soc.*, 2000, **83**, 2721.
8 R. D. Shannon, *J. Appl. Phys.*, 1993, **73**, 348.
9 X. L. Wang, H. Wang and X. Yao, *J. Am. Ceram. Soc.*, 1997, **80**, 2745.
10 D. Zhou, H. Wang, X. Yao and L. X. Pang, *Ceram. Int.*, 2008, **34**, 901.
11 L. Tong, A. Iwase, A. Nattestad, U. Bach, M. Weidelener, G. Götz, A. Mishra, P. Bäuerle, R. Amal, G. G. Wallace and A. J. Mozer, *Energy Environ. Sci.*, 2012, **5**, 9472.
12 J. D. Bierlein and A. W. Sleight, *Solid State Commun.*, 1975, **16**, 69.
13 R. M. Hazen and J. W. E. Mariathasan, *Science*, 1982, **216**, 991.
14 D. Zhou, W. G. Qu, C. A. Randall, L. X. Pang, H. Wang, X. G. Wu, J. Guo, G. Q. Zhang, L. Shui, Q. P. Wang, H. C. Liu and X. Yao, *Acta Mater.*, 2011, **59**, 1502.
15 D. Zhou, L. X. Pang, H. Wang, J. Guo, X. Yao and C. A. Randall, *J. Mater. Chem.*, 2011, **21**, 18412.
16 D. Zhou, C. A. Randall, H. Wang, L. X. Pang and X. Yao, *J. Am. Ceram. Soc.*, 2010, **93**, 2147.
17 A. W. Sleight and W. J. Linn, *Ann. N. Y. Acad. Sci.*, 1976, **272**, 22.
18 L. H. Brixner, A. W. Sleight and M. S. Licis, *J. Solid State Chem.*, 1972, **5**, 247.
19 W. Jeitschko, *Acta Crystallogr., Sect. B: Struct. Crystallogr. Cryst. Chem.*, 1973, **29**, 2074.
20 A. W. Sleight, K. Aykan and D. B. Rogers, *J. Solid State Chem.*, 1975, **13**, 231.
21 F. Theobald, A. Laarif and A. W. Sleight, *Mater. Res. Bull.*, 1985, **20**, 653.
22 F. D. Hardcastle and I. E. Wachs, *J. Phys. Chem.*, 1991, **26**, 10763.
23 A. V. Ghule, K. A. Ghule, S. H. Tzing, J. Y. Chang, H. Chang and Y. C. Ling, *Chem. Phys. Lett.*, 2004, **383**, 208.
24 T. Ono, N. Ogata and R. L. Kuczkowski, *J. Catal.*, 1998, **175**, 185.